Research Paper

Journal of Engineering and Technological Sciences

A Comparative Study of Solid-State and Co-precipitation Methods for Synthesis of NMC622 Cathode Material from Spent Nickel Catalyst

Endah Retno Dyartanti[1,2,*], Tika Paramitha[1,2], Arif Jumari[1,2], Agus Purwanto[1,2], Adrian Nur[1,2], Anatta Wahyu Budiman[1] & Shofirul Sholikhatun Nisa[2]

[1]Department of Chemical Engineering, Universitas Sebelas Maret, Jalan Ir. Sutami No. 36A, Jebres, Surakarta 57126, Indonesia
[2]Centre of Excellence for Electrical Energy Storage Technology, Universitas Sebelas Maret, Jalan Slamet Riyadi No. 435, Laweyan, Surakarta 57146, Indonesia

Corresponding author: endah_rd@staff.uns.ac.id

Abstract

Nickel, the main raw material for lithium-ion batteries (LIB), is currently the most in-demand metal. The rising need for nickel and current environmental concerns have underscored the importance of recycling waste metal to recover its value. Meanwhile, a significant secondary source with a high metal value is spent catalyst. In this context, the acid leaching method was used to recover nickel from spent catalyst. This study aimed to synthesize Lithium Nickel Manganese Cobalt Oxide 622 (NMC622) from spent catalyst. To determine the optimal method, a comparative analysis was conducted between solid-state and co-precipitation methods. Recycled spent nickel catalyst to be used for cathode material was examined by analytical methods, i.e., XRD, FTIR, SEM-EDX, and electrochemical performance testing. The XRD, FTIR, and SEM-EDX tests produced similar outcomes, consistent with previous reports. However, in the electrochemical test, the co-precipitation method showed a specific capacity two times higher than the solid-state method. The NMC622 from the co-precipitation method (NMC622-CP) yielded a specific discharge capacity of 132.82 mAh.g^{-1} at 0.1C, while the retention capacity was 70% for 50 cycles at 0.5C.

Keywords: *cathode material; co-precipitation method; leaching; NMC; recycle; solid-state method; spent catalyst.*

Introduction

Nickel production has been reported to have experienced an annual growth of 3.1% over the last two decades [1-2]. Despite the rising demand, nickel is not a crucial metal due to its availability and worldwide stockpiles, although some potential future uses, including electric vehicles, have been identified [3]. Extracting the metal from primary sources such as mines has significant environmental, social, and economic impacts [4]. In this context, the energy required for nickel production is predicted to contribute substantially to global energy consumption, while environmental implications may increase as production procedures and sites evolve[1, 5].

Spent catalyst can reduce the use of primary resources while providing significant economic benefits[6]. This material results from the catalytic hydroprocessing of petroleum feed that is no longer active. Spent catalyst is prohibited from being disposed of carelessly due to the high levels of harmful metals. Hence, recovery to prevent waste accumulation is a crucial topic[7]. The acid leaching method is the most effective for recovering precious metals in spent catalyst. While both organic and inorganic acids have been studied intensively for this purpose, inorganic acids are not recommended due to the high corrosive potential and toxicity to humans despite their high recovery efficiency. Organic acids, conversely, are considered lighter, have been proven effective in metal recovery, have low corrosive potential, do not produce toxic gases, and can be operated at atmospheric temperatures and pressures [8]. For example, citric acid is a frequently used organic acid for metal extraction from spent catalyst. Each mole of the solution produces three moles of H^+, which is sufficient for metal

ISSN: 2337-5779
J. Eng. Technol. Sci. Vol. 55, No. 5, 2023, 548-557
DOI: 10.5614/j.eng.technol.sci.2023.55.5.4

DOI: 10.5614/j.eng.technol.sci.2023.55.5.4

extraction. In addition, the tricarboxylic nature of citric acid leads to the supply of three carboxylic groups for one mole of acid, resulting in a greater leaching yield [9].

The recovered nickel is mixed with lithium, manganese, and cobalt to form Lithium Nickel Manganese Cobalt Oxide (NMC). This composition provides high specific capacity, great stability, and low internal resistance for lithium-ion batteries[4]. Furthermore, the type of cathode suitable for this combination is NMC622, which has a nickel-manganese-cobalt ratio of 6:2:2[10, 11]. Two methods, solid-state and co-precipitation, are often used for NMC synthesis. The solid-state method is the simplest and can be adapted for large-scale production, but the homogeneity is low and requires a long high-temperature heating time[12, 13]. The second method, co-precipitation, has high homogeneity, tap density, and a spherical particle morphology but demands complex parameter control and has large water requirements [13]. Therefore, this study investigated spent catalyst to be used for lithium-ion battery cathode material, with nickel recovered through citric acid leaching and further processing by comparing two different methods to produce NMC622, namely solid-state and co-precipitation.

Materials and Methods

Materials

The main raw materials used in this study were spent catalyst (PT. Petro Oxo Nusantara), manganese sulfate monohydrate (technical grade), cobalt sulfate heptahydrate (Rubamin, India), and lithium carbonate (Sichuan Brivo Lithium Material Co., Ltd.) as sources of Ni, Mn, Co, and Li. Furthermore, the supporting materials were citric acid monohydrate (technical grade), hydrogen peroxide (50%, technical grade), oxalic acid dihydrate (technical grade), and sodium hydroxide (technical grade). All raw materials, except the spent catalyst, were used directly without treatment and purification.

Methods

Spent Catalyst Leaching

The spent catalyst was ground and sieved with a size of 100 mesh, then a 1 M citric acid solution was prepared and heated to 80 °C. After reaching the desired temperature, the fine spent catalyst was added to the citric acid solution at a ratio of 20 g/L. A reducing agent was further added to the mixture at 3%v/v. During the process, the temperature was maintained at 80 °C for 3 hours. Subsequently, the leachate solution formed was filtered to separate the solution and the residue.

Synthesis of NMC622 by Solid-state Method (NMC622-SS)

The leaching solution obtained in the previous step was precipitated using oxalic acid. Initially, sodium hydroxide was added to the leaching solution to obtain a pH of 7. About 1 M oxalic acid solution was then added to the mixture to reach a pH of 2, followed by heating to 60 °C for 2 hours. Manganese oxalate and cobalt oxalate were also prepared as follows. Manganese sulfate monohydrate and cobalt sulfate heptahydrate were dissolved in 1 M distilled water, respectively. Following this, about 1 M oxalic acid solution was added to each solution and heated at 60 °C for 2 hours. The three precipitates obtained were washed, filtered, and dried in an oven to form nickel, manganese, and cobalt oxalate powders. The next process was solid-state lithiation carried out by adding excess lithium carbonate to a mixture of the three oxalates (Ni-Mn-Co ratio = 6:2:2). The mixture was transferred to a crucible, calcined at 500 °C for 6 hours and sintered at 850 °C for 12 hours. Subsequently, the formed NMC622-SS product was ground and sieved with 200 mesh.

Synthesis of NMC622 by Co-precipitation Method (NMC622-CP)

The leaching solution produced in the previous stage was added with manganese sulfate monohydrate and cobalt sulfate heptahydrate (Ni-Mn-Co ratio = 6:2:2). After the mixture was dissolved, sodium hydroxide solution was added to reach a pH of 7. About 1 M oxalic acid solution was added to attain a pH of 2 while stirring, followed by heating at 60 °C for 2 hours. The precipitate formed was washed, filtered, and dried in an oven to form NMC622 precursor. The next process was lithiation carried out by adding excess lithium carbonate to the

NMC622 precursor. The mixture was transferred to a crucible, calcined at 500 °C for 6 hours, and sintered at 850 °C for 12 hours. Finally, the formed NMC622-CP product was ground and sieved with 200 mesh.

Materials Characterization and Electrochemical Performance

Material characterizations in this study included atomic absorption spectrometry (AAS), X-ray diffraction (XRD), Fourier transform infra-red (FTIR) spectroscopy, thermogravimetric analysis (TGA), and scanning electron microscope-energy dispersive X-ray (SEM-EDX) spectroscopy. AAS (AA-7000 series, Shimadzu, Japan) was used to detect the elements in the liquid samples, specifically nickel. XRD (EQ-MD-10 precision mini XRD, MTI, America) was used to determine the crystal structure and crystal size at 2ɵ using CuKα radiation with λ = 1.5406. FTIR (Shimadzu FTIR Spectrometer, Japan) spectroscopy detected different functional groups in samples in the 4000 to 400 cm^{-1} wavenumber range and TGA (DTG-60, Shimadzu, Japan) measured thermal stability as well as volatile content. Meanwhile, SEM-EDX (Jeol JSM-6510LA, Japan) was used to determine the morphology and composition of the elements in the material.

Electrochemical performance testing commenced with manufacturing NMC622-SS and NMC622-CP cathode sheets. Both powders were added with carboxymethyl cellulose (CMC), acetylene black (AB), styrene-butadiene rubber (SBR), and distilled water to form a slurry, respectively. The slurry was subsequently coated on aluminum foil and dried in the oven, with the coating covering both sides to become cathode sheets. The cathode and anode sheets, separated by a polypropylene separator, were assembled into cylindrical cells. $LiPF_6$ electrolyte (EC-EMC = 3:7) was injected into the cylindrical cell and closed. Electrochemical testing was carried out with a NEWARE Battery Analyzer and the BTS Software.

Result and Discussion

Spent catalyst that lost its catalytic function can be hydrometallurgically processed through acid leaching. The material contains more than 50% Ni and previous studies have reported functional group and composition analyses [14,15]. The nickel content is in the form of nickel oxide (NiO) [15], hence, the leaching process with citric acid and reducing agent results in the following reaction:

$$3NiO_{(s)} + 2C_6H_8O_{7(aq)} + 2H_2O_{2(aq)} \rightleftharpoons C_{12}H_{10}Ni_3O_{14(aq)} + 5H_2O_{(l)} + O_{2(g)} \quad (1)$$

The reaction occurs under the mechanism of acidolysis and complexolysis. In acidolysis, the metal in spent catalyst is protonated, leading to dissolution. Acids dissociate and release protons during acidolysis, causing the removal of the metal from the surface of the spent catalyst according to Eq. (1). Protons (H^+) protonates the anions of insoluble metal compounds such as O_2 in metal oxides (MO). Organic acids extract metals to form soluble complexes through complexation (ligand formation) of previously leached metals [7]. Simultaneously, reducing agents play a role in increasing the leaching rate and the recovery efficiency [16,17]. Nickel citrate complex solution was analyzed using AAS and yielded 90% Ni recovery. This value was used to calculate the Mn and Co requirements for the NMC622 mixture.

Material Characterization

Material characterization was carried out to determine the structure, functional groups, morphology, and composition using XRD, FTIR, and SEM-EDX analysis. The XRD analysis of the nickel oxalate dihydrate and the NMC622 precursor is presented in Fig. 1a. The crystal structure of the sample synthesized from the leaching solution corresponded to the *β*-orthorhombic phase of $NiC_2O_4.2H_2O$ with space group Cccm. The lattice parameter values included, a = 11.902, b = 5.418, and c = 15.494, corresponded to Lopez *et al.* (2013), who obtained values of a = 11.876, b = 5.339, and c = 15.659 [18]. The NMC622 precursor showed the presence of a $NiMnCoC_2O_4.2H_2O$ crystal structure, which also had an *β*-orthorhombic phase with a lattice parameter of a = 11.909, b = 5.423, and c = 15.474. Based on the diffraction pattern, the NMC622 precursor showed broad diffraction peaks as co-effect of its Ni, Mn, and Co composition [19]. In addition, the interaction between X-rays from the Cu and NMC samples caused a fluorescent effect, resulting in noisy XRD patterns [11]. Both samples

DOI: 10.5614/j.eng.technol.sci.2023.55.5.4

were found to have metal-oxalate, which could be directly used as raw material for cathodes by simple heat treatment.

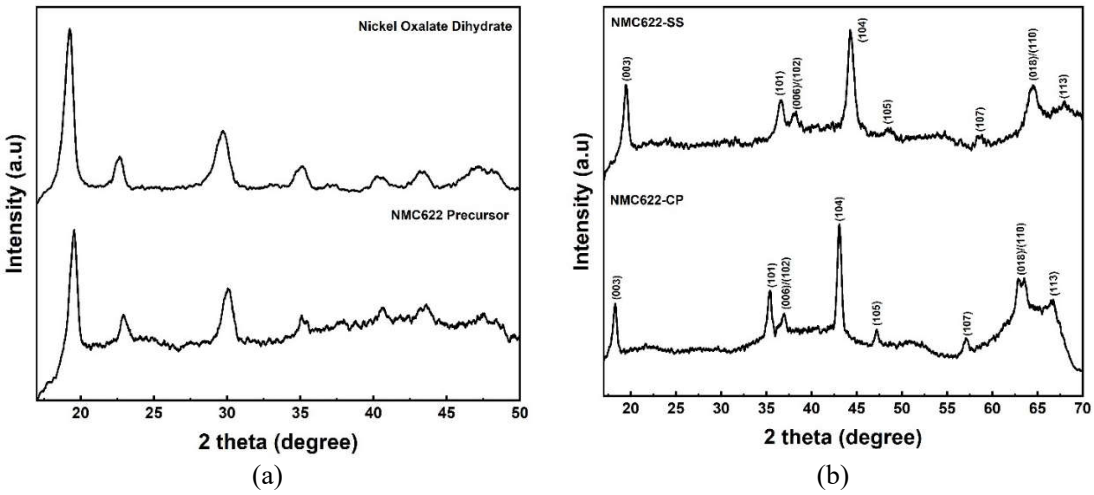

Figure 1 X-ray diffraction peaks (a) before, and (b) after calcination and sintering.

Figure 1b shows samples that have been lithiated and heated, both having a hexagonal α-$NaFeO_2$ structure with an *R3m* space group. Li ions, transition metals, and oxygen ions were presumed to occupy the 3a, 3b, and 6c sites [21]. The structural stability and electrochemical performance of NMC material is known to be influenced by Li^+/Ni^{2+} mixing [22]. Furthermore, a diffraction angle (2θ) of 20° to 35°, a potential surface impurity zone of LiOH and Li_2CO_3, is commonly encountered in high nickel material [23]. Based on the result, there were no detectable surface impurities in any of the examined materials. Sharp and clear diffraction peaks were observed in both samples, suggesting the cathode obtained was well-crystallized. In addition, the peaks in diffraction angle 2θ were similar to those reported in the literature [21,24,25]. The splitting peaks (006)/(102) and (108)/(110) in NMC622-CP were clearer than in NMC622-SS, further confirming that NMC622-CP had a higher layered structure. The low homogeneity of NMC622-SS was largely responsible for the disordered layer structure. The crystal structure of the material was determined using the least squares regression method; the lattice parameters obtained are listed in Table 1. All of the discovered materials had high similarity in lattice characteristics, showing a similar chemical composition. Furthermore, the calculated c/a ratio values for all samples were greater than 4.899, confirming the presence of layered-structure cathode material [26]. NCM622-CP had a lower peak angle (003) than NMC622-SS, showing a larger unit cell c-lattice, which may suggest a broader plane distance for Li^+ mobility during charge and discharge [23].

Table 1 Lattice parameter.

Sample	a (Å)	c (Å)	c/a
NMC622-SS	2.8749	14.0859	4.8996
NMC622-CP	2.9748	14.6333	4.9190

The IR spectra analysis used to determine the absorbance band of the material is presented in Figure 2. The analysis was carried out in the mid-region of 4000 to 400 cm^{-1}. The absorbance band between 600 and 400 cm^{-1} showed the M-O vibration band (M = Ni, Mn, Co), which is characteristic of layered oxides [27,28]. In Fig. 2a, Ni-O bonds were found in both samples at 486 cm^{-1} [28]. C-O bonds were found in the band from 740 to 817 cm^{-1} for the NMC622 precursor, from 780 to 844 cm^{-1} for the $NiC_2O_4.2H_2O$, and from 1312 to 1357 cm^{-1} for both samples. In addition, O-H bonds were also found in the bands 1613 cm^{-1} and 3367 cm^{-1} for the $NiC_2O_4.2H_2O$, and 1613 cm^{-1} and 3380 cm^{-1} for the NMC622 precursor. The carbonate and hydroxide bonds indicate that the sample formed contained oxalate compound.

In Figure 2b, the bands at 486 cm^{-1}, 519 cm^{-1}, and 571 cm^{-1} represent Ni-O stretching mode, Mn-O bending mode, and Co-O, respectively [28]. The three peaks confirm that the material formed contained Ni, Mn, and Co. Compared to Figure 2a, some O-H bond peaks were lost due to heating. However, the O-H peak was still found in the NMC622-SS sample in the 3640 cm^{-1} band, indicating that water compound was still trapped in the material [29]. Furthermore, both samples had C-O peaks in the 870 cm^{-1} and 1460 cm^{-1} bands. The presence of this carbonate bond is caused by Li_2CO_3 [30]. Water provides H^+, generating OH^- that mixes with Li^+ to produce LiOH. LiOH reacts with carbon dioxide in the atmosphere to generate Li_2CO_3 [31].

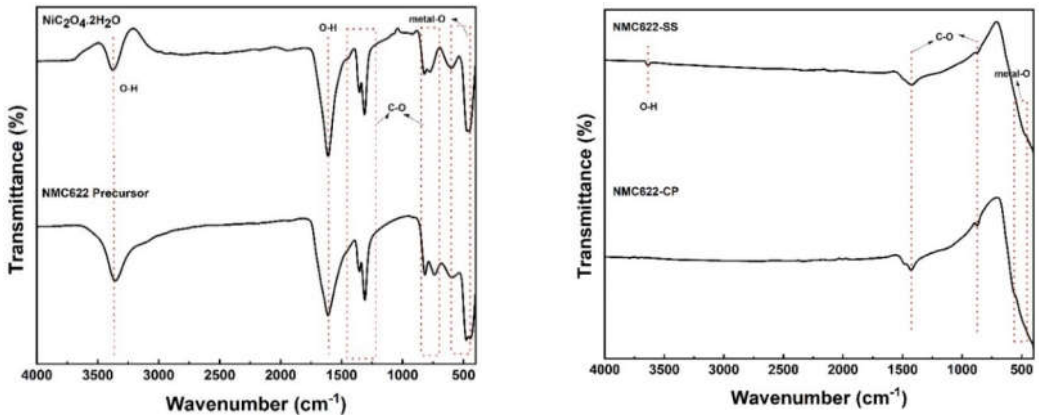

Figure 2 The IR spectra (a) before, and (b) after calcination and sintering.

Thermal analysis was carried out to measure the thermal stability and volatile content of the material at a temperature range of 30 to 900 °C. The loss on ignition was computed using the mass change before and after the reaction [32]:

$$\text{Ignition loss} = 1 - \text{productivity} \quad (2)$$

At 75 to 150 °C, Figure 3 shows a slight decrease in the curve attributed to the evaporation of organic matter. As the temperature continued to rise, decomposition occurred and the rate increased with higher temperature. A more significant decrease was observed in the curve at a temperature of 178 to 274 °C, showing the loss of water adsorbed on the surface of the sample. This reduction of some water and alcohol molecules resulted in a weight loss of 14.53%. At a temperature of 275 to 650 °C, another 38.59% of weight loss occurred due to the internal reaction of lithium, nickel, manganese, and cobalt oxides, thereby confirming the formation of NMC crystals [33]. Both samples had a total weight reduction of 53.12%, consistent with the computation equation (2), which is based on the expected weight loss of 53.25%.

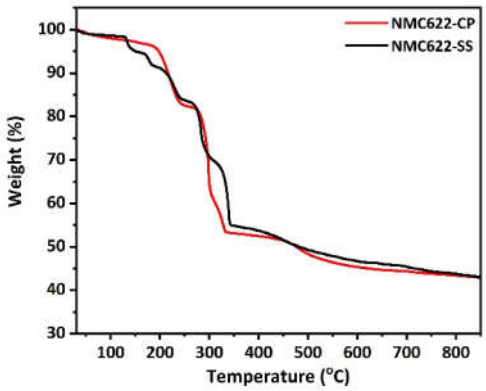

Figure 3 Thermal analysis of NMC622-SS and NMC622-CP.

DOI: 10.5614/j.eng.technol.sci.2023.55.5.4

The morphology of NMC622-SS and NMC622-CP at 500x and 5000x magnification is presented in Figure 4. All samples had inhomogeneous particle shapes. The primary particles agglomerated to form secondary particles, whereas NMC622-CP had smaller secondary particles than NMC622-SS. The primary particle size distribution is shown in the histogram in Figure 5. Both samples had average submicron-sized primary particles of 0.581 µm and 0.761 µm for NMC622-CP and NMC622-SS, respectively. It can be seen that the particle size of NMC622-CP was more uniform compared to that of NMC622-SS. The tap density of NMC622-SS and NMC622-CP was not much different at 0.858 $g.cm^{-3}$ and 0.872 $g.cm^{-3}$, respectively. Then, the surface areas of both were 2.978 $m^2.g^{-1}$ and 3.868 $m^2.g^{-1}$ for NMC622-SS and NMC622-CP, respectively. This particle size affects the electrochemical performance of the material, which will be explained later. To study the elemental distribution, the EDX analysis gave the results shown in Table 2. Both samples were close to the nominal ratio of Ni-Mn-Co = 6:2:2.

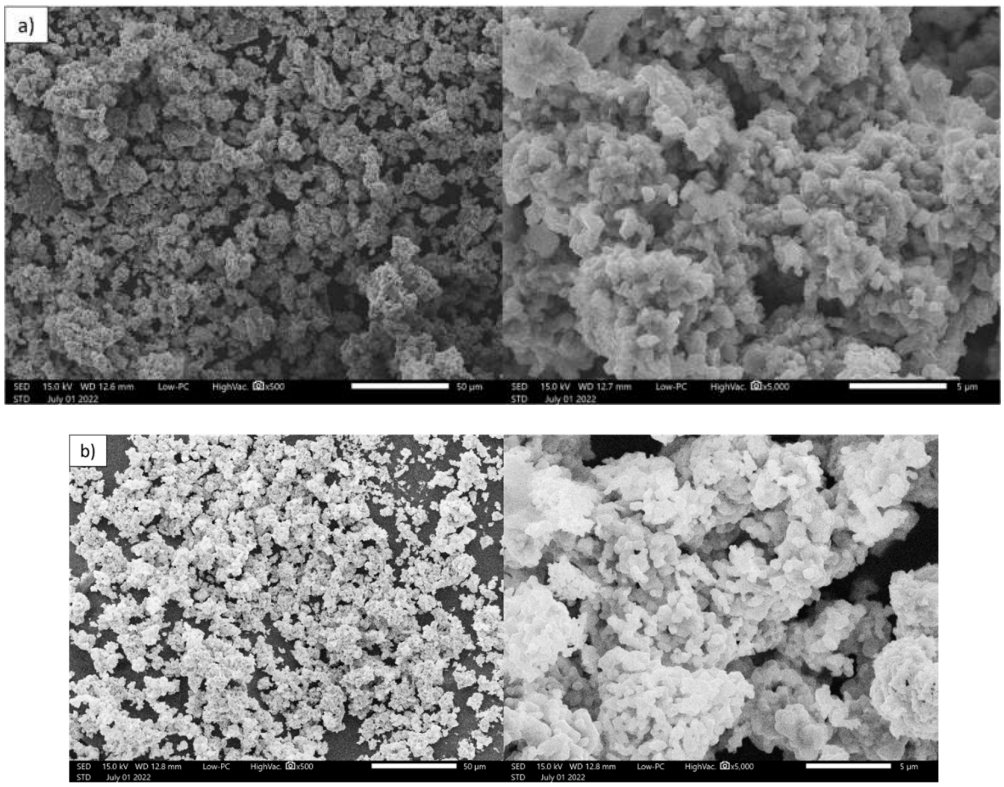

Figure 4 SEM image of (a) NMC622-SS and (b) NMC622-CP.

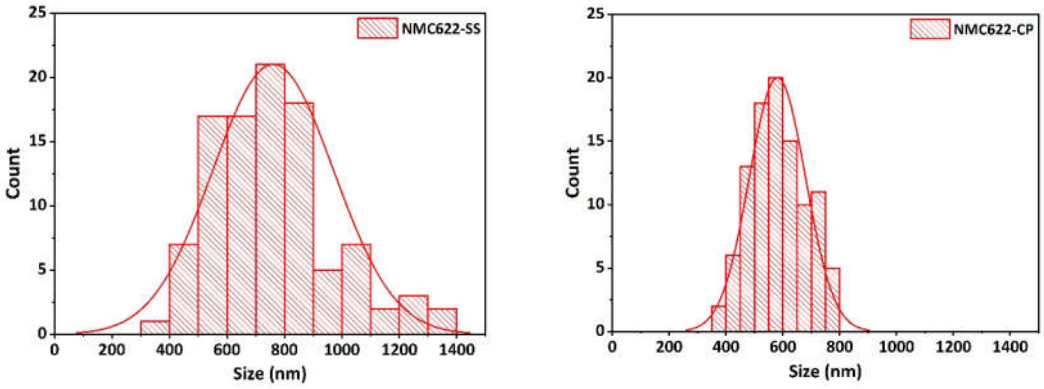

Figure 5 Particle size histogram.

Table 2 EDX results of the samples.

Sample	Ni (Atom%)	Mn (Atom%)	Co (Atom%)
NMC622-SS	59.6	21.0	19.4
NMC622-CP	59.7	22.9	17.4

Electrochemical Performance

An electrochemical test was conducted to examine the basic parameters and show the effectiveness of the proposed methods in fabricating NMC622 cathode material from spent catalyst. For this purpose, galvanostatic charge-discharge experiments were carried out with different C-rates to determine NMC cathode capacity, rate capability, and cycling stability. All cells were assembled into cylindrical cells with graphite as anode, and a charged-discharged range of 4.3 V to 2.5 V. Figure 6a showed that the first cycle-specific discharge capacities of NMC622-SS and NMC622-CP were 68.22 mAh.g^{-1} and 132.82 mAh.g^{-1} at a rate of 0.1C, respectively. NMC622-CP provided a higher specific discharge capacity due to its smaller particle size compared to NMC622-SS. An increase in the surface area to volume ratio resulted in shorter intraparticle diffusion routes and greater use of each particle. Consequently, more active material was used because Li^+ diffused more easily across smaller particles [34]. The curves of the first five and tenth cycles of NMC622-CP are shown in Figure 6b. Initial charge-discharge curve instability is related to solid electrolyte interface (SEI) formation. Li was deposited on the anode surface during discharge, thereby blocking the return to cathode [35]. After three cycles, the curve appeared to be constant due to the relatively stable SEI formed [36]. SEI maintains cycle stability and prevents degradation of cathode, acting as a protective film [37].

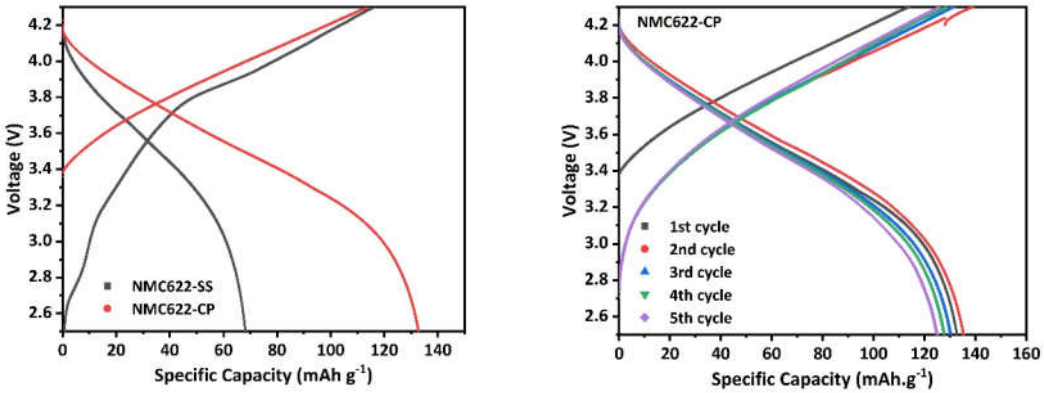

Figure 6 Charge-discharge curves of (a) the 1st cycle of NMC622-SS and NMC622-CP at 0.1C and (b) the 1st to the 10th cycle of NMC622-CP at 0.1C.

Given that NMC622-CP provided a specific capacity twice larger than NMC622-SS, it was tested for rate-ability and cycle-ability as presented in Figure 7. In Figure 7a, NMC622-CP shows a specific discharge capacity of 108.23 mAh.g^{-1} at 0.5C, which decreased after 50 cycles to 75.72 mAh.g^{-1}. The retention capacity of the discharge was 70%, showing relatively lower stability caused by a substantial decline. The capacity increased slightly every few cycles due to the SEI layer formed on the surface of the electrode during the initial cycle. As the SEI layer expanded and stabilized during the first few cycles, a gradual capacity increase occurred [37]. This phenomenon was also subject to the influence of poor surrounding temperature control [38,39]. As shown by real-time data from charge-discharge tests, the discharge capacity decreased when the air temperature dropped at night. Meanwhile, with increasing air temperatures during the day, the discharge capacity increased. Based on the result, a discharge capacity of 64.02 mAh.g^{-1} at the highest level of 1C was obtained, showing effective performance within such a discharge protocol. Subsequently, it regained a capacity of 96.93 mAh.g^{-1} at 0.1C, as presented in Fig. 7b. The relatively low retention capacity of NMC622-CP was due to the use of water as solvent for the cathode slurry. Water exposure decreases surface pollutants and leaches Li^+, which presumably re-

DOI: 10.5614/j.eng.technol.sci.2023.55.5.4

deposits upon drying. Minor surface differences may promote higher Li loss and transition metal dissolution during the cycle, causing capacity fading [31].

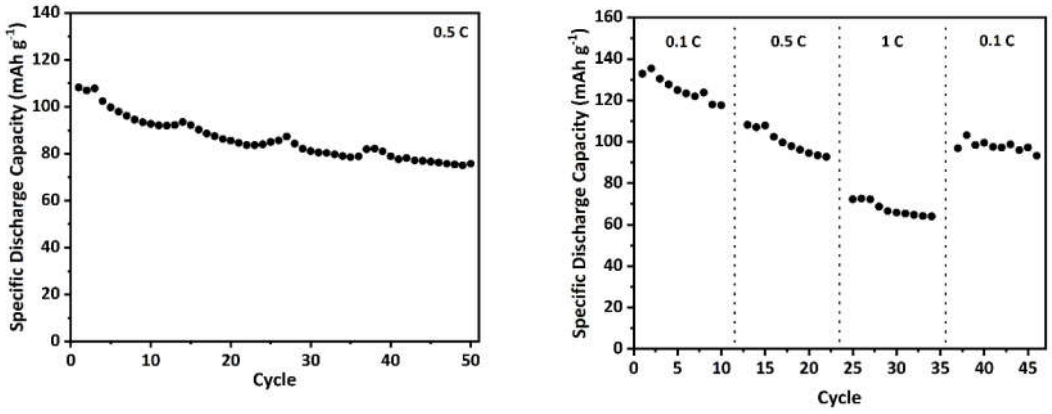

(a) (b)

Figure 7 (a) Cycle-ability at 0.5C and (b) rate-ability of NMC622-CP

Conclusion

In conclusion, this study successfully synthesized NMC622 cathode material from spent catalyst prepared by acid leaching to recover Ni. Leaching solution containing Ni was processed by two methods, namely solid-state (NMC622-SS) and co-precipitation (NMC622-CP). The results of material characterization and electrochemical performance were consistent with those from previous reports. Both samples had a layered hexagonal structure, and no impurities were detected. NMC622-CP provided two times higher specific discharge capacity (132.82 $mAh.g^{-1}$) than NMC62-SS. Furthermore, NMC622-CP was measured at C-rates up to 1C with a specific discharge capacity almost the same as NMC622-SS at 0.1C. Based on the results, the co-precipitation method was considered the most suitable method in this study. NMC622-CP sample provided capacity retention of 70%, which is still low for Li-ion battery applications. Therefore, further studies are needed to improve the performance stability of the NMC622 cathode material.

Acknowledgement

This study was funded by the Non-APBN Universitas Sebelas Maret fund through the *Hibah Grup Riset* scheme (Contract Number: 254/UN27.22/PT.01.03/2022).

References

[1] Elshkaki, A., Graedel, T.E., Ciacci, L. & Reck, B.K., *Resource Demand Scenarios for the Major Metals*, Environmental Science and Technology, **52**(5), pp. 2491–2497, Feb. 2018.

[2] Henckens, M.L.C.M. & Worrell, E., *Reviewing the Availability of Copper and Nickel for Future Generations. The balance between Production Growth, Sustainability and Recycling Rates*, Journal of Cleaner Production, **264**, 121460, Mar. 2020.

[3] Habib, K., Hansdóttir, S.T. & Habib, H., *Critical Metals for Electromobility: Global Demand Scenarios for Passenger Vehicles, 2015–2050*, Resources, Conservation and Recycling, **154**, 104603, Jun. 2020.

[4] Murdock, B.E., Toghill, K.E. & Tapia-Ruiz, N., *A Perspective on the Sustainability of Cathode Materials used in Lithium-Ion Batteries*, Advanced Energy Materials, **11**(39), 2021.

[5] Guohua, Y., Elshkaki, A. & Xiao, X., *Dynamic Analysis of Future Nickel Demand, Supply, and Associated Materials, Energy, Water, and Carbon Emissions in China*, Resources Policy, **74**, 102432, Sept. 2021.

[6] Erust, C., Akcil, A., Bedelova, Z., Anarbekov, K., Baikonurova, A. & Tuncuk, A., *Recovery of Vanadium from Spent Catalysts of Sulfuric Acid Plant by using Inorganic and Organic Acids: Laboratory and Semi-pilot tests*, Waste Management, **49**, pp. 455-461, Dec. 2016.

[7] Pathak, A., Vinoba, M. & Kothari, R., *Emerging Role of Organic Acids in Leaching of Valuable Metals from Refinery-spent Hydroprocessing Catalysts, and Potential Techno-economic Challenges: A Review*, Critical Reviews in Environmental Science and Technology, **51**(1), pp. 1-43, Jan. 2020.

[8] Al-Sheeha, H., Marafi, M., Raghavan, V. & Rana, M., *Recycling and Recovery Routes for Spent Hydroprocessing Catalyst Waste*, Industrial and Engineering Chemistry Research, **52**(36), pp. 12794-12801, Aug. 2013.

[9] Golmohammadzadeh, R., Rashchi, F. & Vahidi, E., *Recovery of Lithium and Cobalt from Spent Lithium-ion Batteries Using Organic Acids: Process Optimization and Kinetic Aspects*, Waste Management, **64**, pp. 244-254, Mar. 2017.

[10] Kasnatscheew, J., Evertz, M., Kloepsch, R., Streipert, B., Wagner, R., Laskovic, I.C. & Winter M., *Learning from Electrochemical Data: Simple Evaluation and Classification of LiMO2-type-based Positive Electrodes for Li-Ion Batteries*, Energy Technology, **5**(9), pp. 1670-1679, 2017.

[11] Nisa, S.S., Rahmawati, M., Yudha, C.S., Nilasary, H., Nursukatmo, H., Oktaviano, H.S., Muzayanha, S.U. & Purwanto, A., *A Fast Approach to Obtain Layered Transition-Metal Cathode Material for Rechargeable Batteries*, Batteries **8**(1), Jan. 2022.

[12] Malik, M., Chan, K.H. & Azimi, G., *Effect of Synthesis Method on the Electrochemical Performance of LiNixMnCo1-x-yO2 (NMC) Cathode for Li-Ion Batteries: A Review*, G. Azimi et al. (eds.), *Rare Metal Technology 2021*, The Minerals, Metals and Materials Series, pp. 37-46, 2021.

[13] Purwanto, A., Yudha, C.S., Ubaidillah, U., Widiyandari, H., Ogi, T., & Haerudin, H., *NCA cathode material: Synthesis methods and performance enhancement efforts*, Materials Research Express, **5**(12), pp. 122001, 2018.

[14] Nisa, S.S., Nurohmah, A.R., Yudha, C.S., Nilasary, H., Nursukatmo, H., Dyartanti, E.R. & Purwanto, A., *Utilization of Spent Nickel Catalyst as Raw Material for Ni- Rich Cathode Material*, Jurnal Presipitasi, **18**(2), pp. 349-357, 2021.

[15] Nisa, S.S., Nurohmah, A.R., Yudha, C.S., Rahmawati, M., Paramitha, T., Widiyandari, H., Dyartanti, E.R. & Purwanto, A., *Preliminary Investigation of NiO Anode for NCA/NiO Battery from Spent Catalyst Recovery,* IOP Conference Series: Materials Science and Engineering, **1096**, 012140, 2021.

[16] Gao, W., Song, J., Cao, H., Lin, X., Zhang, X., Zheng, X., Zhang, Y. & Sun, Z., *Selective Recovery of Valuable Metals from Spent Lithium-ion Batteries – Process Development and Kinetics Evaluation*, Journal of Cleaner Production, **178**, pp. 833-845, Jan. 2018.

[17] Jumari, A., Yudha, C.S., Nizam, M., Dyartanti, E.R., Suranto & Purwanto, A., *An Environmentally Friendly Hydrometallurgy Process for the Recovery and Reuse of Metals from Spent Lithium-ion Batteries, using Organic Acid*, Open Engineering, **12**(1), pp. 485-494, Jun. 2022.

[18] López, M.C., Tirado, J.L. & Vicente, C.P., *Structural and Comparative Electrochemical Study of M(II) Oxalates, M = Mn, Fe, Co, Ni, Cu, Zn*, Journal of Power Sources, **227**, pp. 65-71, Aug. 2013.

[19] Yang, Z., Lu, J., Bian, D., Zhang, W., Yang, X., Xia, J., Chen, G., Gu, H. & Ma, G., *Stepwise Co-precipitation to Synthesize LiNi1/3Co1/3Mn1/3O2one-dimensional Hierarchical Structure for Lithium Ion Batteries*, Journal of Power Sources, **272**, pp. 144-151, Aug. 2014.

[20] Refly, S., Floweri, O., Mayangsari, T.R., Aimon, A.H. & Iskandar, F., *Green Recycle Processing of Cathode Active Material from LiNi1/3Co1/3Mn1/3O2(NCM 111) Battery Waste through Citric Acid Leaching and Oxalate Co-precipitation Process*, Materials Today: Proceedings, **44**, pp. 3378–3380, Nov. 2020.

[21] Li, H., Li, J., Ma, X. & Dahn, J.R., *Synthesis of Single Crystal LiNi 0.6 Mn 0.2 Co 0.2 O 2 with Enhanced Electrochemical Performance for Lithium Ion Batteries*, Journal of The Electrochemical Society, **165**(5), pp. A1038–A1045, 2018.

[22] Wang, R., Qian, G., Liu, T., Li, M., Liu, J., Zhang, B., Zhu, W., Li, S., Zhao, W., Yang, W., Ma, X., Fu, Z., Liu, Y., Yang, J., Jin, L., Xiao, Y. & Pan, F., *Tuning Li-enrichment in High-Ni layered Oxide Cathodes to Optimize Electrochemical Performance for Li-ion Battery*, Nano Energy, **62**, pp. 709-717, May. 2019.

DOI: 10.5614/j.eng.technol.sci.2023.55.5.4

[23] Zhang, N., Li, Y. & Qiao, Y., *Boosting the Electrochemical Performance of $LiNi_{0.6}Mn_{0.2}Co_{0.2}O_2$ through a Trace Amount of Mg-B Co-doping*, Journal of Materials Science and Technology, **89**, pp. 167-178, Feb. 2021.

[24] Zybert, M., Ronduda, H., Szczęsna, A., Trzeciak, T., Ostrowski, A., Żero, E., Wieczorek, W., Rarog-Pilecka, W. & Marcinek, M., *Different Strategies of Introduction of Lithium Ions into Nickel-manganese-cobalt Carbonate Resulting in LiNi0.6Mn0.2Co0.2O2 (NMC622) Cathode Material for Li-ion Batteries*, Solid State Ionics, **348**, 115273, Feb. 2020.

[25] Lipson, A.L., Durham, J.L., Leresche, M., Abu-Baker, I., Murphy, M.J., Fister, T.T., Wang, L., Zhou, F., Liu, L., Kim, K. & Johnson, D., *Improving the Thermal Stability of NMC 622 Li-Ion Battery Cathodes through Doping during Coprecipitation*, ACS Applied Materials and Interfaces, **12**(16), pp. 18512-18518, Apr. 2020.

[26] Zhu, J., Vo, T., Li, D., Lu, R., Kinsinger, N.M., Xiong, L., Yan, Y. & Kisailus, D., *Crystal Growth of Li $[Ni_{1/3}Co_{1/3}Mn_{1/3}]O_2$ as a Cathode Material for High-Performance Lithium Ion Batteries*, Crystal Growth & Design, **12**(3), pp.1118-1123, Des. 2012.

[27] Cho, Y., Lee, M.H., Kim, H., Ku, K., Yoon, G., Jung, S.K., Lee, B., Kim, J. & Kang, K., *Activating Layered $LiNi_{0.5}Co_{0.2}Mn_{0.3}O_2$ as a Host for Mg Intercalation in Rechargeable Mg Batteries*, Materials Research Bulletin, **96**, pp. 524-532, Apr. 2017.

[28] Zhou, H., Zhao, X., Yin C. & Li, J., *Regeneration of $LiNi_{0.5}Co_{0.2}Mn_{0.3}O_2$ Cathode Material from Spent Lithium-ion Batteries*, Electrochimica Acta, **291**, pp. 142–150, 2018.

[29] Castellanos-Leal, E.L., Acevedo-Peña, P., Güiza-Argüello, V.R. & Córdoba-Tuta, E.M., *N and F Codoped TiO2 Thin Films on Stainless Steel for Photoelectrocatalytic Removal of Cyanide Ions in Aqueous Solutions*, Materials Research, **20**(2), pp. 487-495, 2017.

[30] Yudha, C.S., Muzayanha, S.U., Hendri, W., Iskandar, F., Sutopo, W. & Purwanto, A., *Synthesis of $LiNi_{0.85}Co_{0.14}Al_{0.01}O_2$ Cathode Material and its Performance in an NCA / Graphite Full-Battery*, Energies, **12**, 1886, May 2019.

[31] Wood, M., Li, J., Ruther, R.E., Du, Z., Self, E.C., Meyer III, H., Claus, D., Belharouak, I. & Wood III, D.L., *Chemical Stability and Long-term Cell Performance of Low-cobalt, Ni-Rich Cathodes Prepared by Aqueous Processing for High-energy Li-Ion batteries*, Energy Storage Materials, **24**, pp. 188-197, May 2019.

[32] Wang, L., Zhan, Y., Luo, S., Wang, Y., Li, S. & Chang, L., *Preparation and Electrochemical Properties of Cationic Substitution $Li_2Mn_{0.98}M_{0.02}SiO_4$ (M = Mg, Ni, Cr) as Cathode Material for Lithium-ion Batteries*, Ionics (Kiel)., **26**(8), pp. 3769-3775, Mar. 2020.

[33] Aregai, T., Babu, K.V., Babu, B.V. & Veeraiah, V., *Effect of Calcination and Sintering Temperature on the Properties of Layered LiNi 1 / 3 Co 1 / 3 Mn 1 / 3 O 2 Cathode Material for Lithium-ion Batteries*, International Journal of ChemTech Research, **10**(10), pp. 479-489, Oct. 2017.

[34] Wood, M., Li, J., Du, Z., Daniel, C., Dunlop, A.R., Polzin, B.J., Jansen, A.N., Krumdick, G. & Wood III, David L., *Impact of Secondary Particle Size and Two-layer Architectures on the High-rate Performance of Thick Electrodes in Lithium-ion Battery Pouch Cells*, Journal of Power Sources, **515,** 230429, Aug. 2021.

[35] Yudha, C.S., Hutama, A.P., Rahmawati, M., Arinawati, M., Aliwarga, H.K., Widiyandari, H. & Purwanto, A., *Production of Nickel-rich $LiNi_{0.89}Co_{0.08}Al_{0.03}O_2$ Cathode Material for High Capacity NCA/Graphite Secondary Battery Fabrication*, Open Engingeering, **12**(1), pp. 501-510, Apr. 2022.

[36] Joshi, T., Eom, K., Yushin, G., & Fuller, T.F., *Effects of Dissolved Transition Metals on the Electrochemical Performance and SEI Growth in Lithium-Ion Batteries*, Journal of The Electrochemical Society, **161**(12)**,** pp. A1915-A1921, Aug. 2014.

[37] An, S.J., Li, J., Daniel, J., Mohanty, D., Nagpure, S. & Wood, D.L., *The state of Understanding of the Lithium-ion-battery Graphite Solid Electrolyte Interphase (SEI) and Its Relationship to Formation Cycling*, Carbon, **105**, pp. 52–76, Mar. 2016.

[38] Shen, Y., Eltzholtz, J.R. & Iversen, B.B., *Controlling Size, Crystallinity, and Electrochemical Performance of Li 4 Ti 5 O 12 Nanocrystals*, Chemistry of Materials, **25**, pp. 5023–5030, Nov. 2013.

[39] Purwanto, A., Muzayanha, S.U., Yudha, C.S., Widiyandari, H., Jumari, A., Dyartanti, E.R., Nizam, M. & Putra, M.I., *High Performance of Salt-modified–LTO Anode in LiFePO4 Battery*, Applied Sciences, **10**(20), pp. 1-15, 2020.

Manuscript Received: 2 March 2023
1st Manuscript Revision Received: 18 July 2023
2nd Manuscript Revision Received: 12 October 2023
Accepted Manuscript: 14 November 2023